Received: 29 April 2021 | Revised: 2 July 2021 | Accepted: 20 July 2021

DOI: 10.1111/jmi.13052

Journal of Microscopy RMS

ORIGINAL ARTICLE

Using hybrid atomic force microscopy and infrared spectroscopy (AFM-IR) to identify chemical components of the hair medulla on the nanoscale

Alexander P. Fellows | **Mike T. L. Casford** | **Paul B. Davies**

Department of Chemistry, University of Cambridge, Cambridge, UK

Correspondence
Alexander P. Fellows, Department of Chemistry, University of Cambridge, Lensfield Road, Cambridge CB2 1EW, UK.
Email: apf36@cam.ac.uk

Abstract

Atomic force microscopy integrated with infrared spectroscopy (AFM-IR) has been used to topographically and chemically examine the medulla of human hair fibres with nanometre scale lateral resolution. The mapping of cross-sections of the medulla showed two distinct structural components which were subsequently characterised spectroscopically. One of these components was shown to be closely similar to cortical cell species, consistent with the fibrillar structures found in previous electron microscope (EM) investigations. The other component showed large chemical differences from cortical cells and was assigned to globular vacuole species, also confirming EM observations. Further characterisation of the two components was achieved through spectral deconvolution of the protein Amide-I and -II bands. This showed that the vacuoles have a greater proportion of the most thermodynamically stable conformation, namely the antiparallel β-sheet structures. This chimes with the observed lower cysteine concentration, indicating a lower proportion of restrictive disulphide cross-link bonding. Furthermore, the large α-helix presence within the vacuoles points to a loss of matrix-like material as well as significant intermolecular stabilisation of the protein structures. By analysing the carbonyl stretching region, it was established that the fibrillar, cortical cell-like components showed considerable stabilisation from H-bonding interactions, similar to the cortex, involving amino acid side chains whereas, in contrast, the vacuoles were found to only be stabilised significantly by structural lipids.

KEYWORDS
AFM-IR, hair, macrofibril, medulla, nanoscale IR mapping, vacuole

1 | INTRODUCTION

The large-scale internal structure of hair fibres is well known, with the central medulla region surrounded by the cortex and the cuticle, and is illustrated in Figure 1 with the aid of microscopy images and schematic representations. Understanding the structure of the medulla, and exactly what it contributes to bulk hair properties is important in several fields from the textile industry to cosmetic applications.[1–6] However, the great amount of

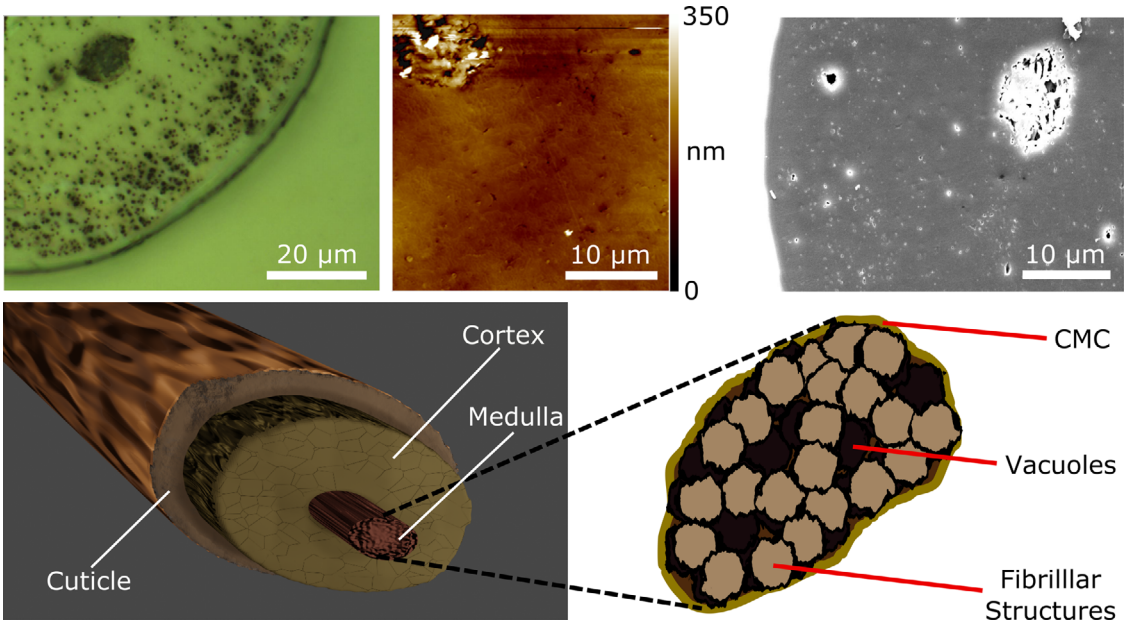

FIGURE 1 Internal structure of a hair fibre showing an optical microscopy image (top left), AFM topography map (top centre) and SEM image (top right), and a schematic of its layered structure (bottom left) and expanded structure of the medulla (bottom right)

research on hair structure over the last century has overlooked the medulla because it was perceived as making little contribution to bulk hair properties.[7–9] The nature of the actual sub-structure of the medulla is controversial. It is commonly considered to consist of vacuolated cells bound together by cell membrane complex (CMC) which, in turn, consists of three distinct layers: two outer, lipid-rich, β-layers sandwiching a central proteinaceous and polysaccharide-rich δ-layer.[10] However, it has recently been suggested that the medulla not only comprises these air-filled vacuoles, but also some of the surrounding components. This suggestion originates from the observation of CMC separating the cortex from a central structure consisting of more than just the vacuolated cells.[11] Alternatively, it has been suggested that the medulla consists of an amorphous material, high in lipid concentration, which produces a porous structure that contains some of the air-filled vacuoles.[12–15] Electron microscopy (both SEM and TEM) shows that the supposed amorphous material comprising the bulk of the medulla is actually fibrillar in structure that is randomly oriented and disorganised.[11,16] These fibrillar structures are believed to be deformed, sparsely packed cortical cells, hence their random orientations and less well-defined structures, bound to the vacuoles through citrulline residue peptide bonds.[17]

The EM observations, therefore, propose that the medulla has three main constituents: globular structures interspersed with fibrillar ones, encompassed by a membrane. The globular structures are assigned to the air-filled vacuoles and often treated as defects within the network of fibrillar cortical cells.[11,12] Due to the presence of the vacuoles, the density of the medulla is low, providing less structural support for the cortical cells, accounting for the large deformations and random orientations that are present. This random distribution of the fibrils, unlike the collateral structure found in the cortex, has a significant effect on the mechanical properties. So although the vacuoles do not actively contribute to the structure or properties of the hair, their presence alters the packing and orientation of the fibrils which play an important role in the mechanical characteristics of hair.[12]

Although it achieves high resolution, EM imaging lacks chemical information which must be inferred indirectly from other techniques like FTIR or Raman. These optical techniques are subject to the diffraction limit of light and hence cannot resolve many of the crucial sub-micron structures that are present in hair. A recent development by Dazzi et al, however, has integrated AFM with an IR laser (AFM-IR) and enables surface-sensitive vibrational spectroscopy at the spatial resolution achievable by AFM (ie nanometre scale).[18] AFM-IR uses the sharp AFM tip to detect any localised photothermal expansion caused by the incident radiation of the IR laser when it is absorbed by vibrational transitions. The application of this technique to hair and other biological surfaces has provided very significant gains in chemical resolution.[19–24] For example, Marcott et al measured the chemical distribution of structural lipids across the complete cross-section of the hair fibre, showing the high lipid concentration present in the medulla and CMC,[25] and Fellows et al have applied the technique to show the sub-structures associated with the cuticle.[26] The current work reports the application of

AFM-IR to the medulla, providing complementary results to electron microscopy for determining its structure, in particular by gaining nanoscale chemical resolution of the different sub-units. This results in a significantly deeper understanding of the nature of the observed constituents.

2 | EXPERIMENTAL

2.1 | Sample preparation

Human hairs (European brown), obtained from multiple individuals, were washed several times with Millipore water and rinsed with methanol. Bundles of approximately 5–10 hairs were embedded in epoxy resin and sectioned into 100, 200 and 300 nm thick cross-sections using a diamond ultramicrotome, generating samples covering different regions of individual hair fibres, as well as a variation across hairs from different individuals. The cross-sections were subsequently positioned, adhesive free, onto glass coverslips for AFM-IR analysis. Several methods for generating these cross-sections were explored, namely, slicing at room temperature using an ultramicrotome and either free, unsupported fibres as well as mounting the fibres in a loose support (plastic pipette tip), or embedding the fibres in a resin support (as above), as well as using a cryo-ultramicrotome to freeze the fibres during sectioning. Of these methods, embedding the fibres in resin proved to be the only reliable way of generating good quality sections at the required thicknesses. At these thicknesses, the major contribution to the AFM-IR signal will arise from the surface layer with gradually diminishing contributions deeper into the sample. In order to assess any axial variability in the cross-section from differing constituents deeper into the sample, spectra from the three different thicknesses were compared, where no significant variation was observed. This is to be expected because the major contributions arising from the surface layer as well as the size of the medulla components being probed being of a similar order to the sample thickness. This results in minimal structural variations throughout the entire depth of sample. Furthermore, the spectra arise from averaging across multiple locations and from several different sections, which minimises the spectral contributions from other structural components that can arise from any axial variability.

The AFM-IR contributions from the underlying glass coverslips were found to be negligible (as expected due to diminishing contributions through the sample depth) by comparing spectra obtained across different sample thicknesses as well as those purely from the glass coverslips. Similarly, any contributions from the epoxy resin were also ruled out due to the clear diminishing IR intensities and changes in physical surface properties due to the epoxy across the cuticle and outer regions of the cortex (ie significant penetration was only found in the outer 3–7 μm and thus considered irrelevant to the medulla).

2.2 | AFM-IR analysis

Spectra and maps were recorded in contact mode using an Anasys NanoIR2 instrument equipped with a MIRcat Laser system (Daylight Solutions) containing four quantum cascade lasers (QCLs) covering the 1125–2298 cm^{-1} spectral range. The AFM cantilever-tip assemblies used were gold-coated with 30 nm tip radius, spring constant 0.07–0.4 Nm^{-1} and resonant frequency 13 ± 4 kHz (Anasys Instruments). Mapping was achieved with a 0.5 Hz scan rate at resolutions of at least 200×200 pixels. IR analysis was done in resonant-enhanced mode (using a 3% duty cycle) with mapping tracking the contact resonance with a PLL (Phase-Locked Loop). The laser power was selected depending on both the sample thickness and observed intensity from the localised region under the tip.

Significant variation was observed for the different localised structures, most likely due to the structural nature of the different components and also tip-sample coupling effects. In order to achieve optimum signal-to-noise ratio spectra whilst avoiding saturation, the thicker samples required between 3%–8% of the available laser power and up to 27% of the laser power for the 100 nm cross-sections in the MD2 regions (defined in the results section). To ensure accurate spectral deconvolution, spectra were recorded at 1 cm^{-1} per point to enable optimum subtraction of sharp water vapour contributions. IR maps were primarily used for identification of the different components to the hair medulla rather than for analysing their individual composition.

Localised AFM-IR point spectra were recorded at locations corresponding to structures in the microscope images that showed similar properties. Due to this localisation, the point spectra could be recorded at positions corresponding to the individual structural components and away from the boundary with other identifiable structures. This, along with averaging across multiple surface locations, minimises any potential spectral contributions from sources in close proximity to the boundary between different structures.

2.3 | Spectral analysis

AFM-IR spectra were recorded under reduced-humidity (dry N_2) to minimise water vapour bands that are prominent in the Amide-I region. (This further enhances the

efficiency of subtracting atmospheric bands.) First, the spectra were automatically background-corrected to remove environmental absorptions and variations in the laser power spectrum. Next, further background subtraction was applied to remove underlying broad spectral variations using a spline curve with subsequent smoothing using a 7 pt low-pass FFT-filter to remove high-frequency noise contributions whilst minimising the effects on the underlying (broader) spectral features. (The effectiveness of this protocol to minimise spectral deviations was critically appraised by comparison with the raw spectra, applying the same procedures used previously.[26]) The smoothing algorithm then enabled quantitative derivative analysis for band-centre identification to be made and accurate spectral deconvolution into the contributing bands.

High confidence in the validity of the deconvolution procedure is based on several factors: first, spectral deviations from the FFT smoothing procedure were monitored to ensure that there were no significant shifts in the underlying band shapes; second, that the derivative analysis identified band contributions at well-known spectral band origins reported in the literature and finally, as expected, deconvoluted bands of species common to both the Amide-I and Amide-II regions showed the same relative intensities. Additional and more detailed information on implementing spectral deconvolution for proteinaceous materials can be found elsewhere.[27–31]

Spectra on a specific hair fibre were recorded with 3–5 co-averages per location and averaged over 15 different surface locations for each section, corresponding to each structure investigated, showing good reproducibility both across the different locations within the same section as well as comparing the average spectra from one section to another from the same hair fibre. Some variability between different fibres (from different individuals) was observed in the absolute spectral contributions, as expected for complex biological samples, yielding quantitative relative intensity variations up to ~10%, and thus leading to more significant differences in the absolute intensity ratios between different spectral bands. However, the relative comparisons between the structures were qualitatively consistent (ie the intensity ratios were consistently above or below unity across different fibres when comparing the same spectral contributions). Although this prohibits a quantitative analysis of the absolute structural determination of the individual medulla constituents, it does allow for qualitative comparisons of the different relative concentrations of structural components that are consistent between different fibres. The spectra and analysis presented here are, therefore, from a representative sample of a hair fibre, averaged across multiple different sections.

2.4 | Similarity index calculation

The similarity index between two spectra was calculated using the normalised sum-of-squares from their difference spectrum which results in identical spectra giving an index of unity and spectra with no overlap similarity resulting in a vanishing index. However, any two spectra that show similar band features, although not from the same source, will still give a non-zero similarity index which might lead to incorrect conclusions. In this work, however, each structure investigated is believed to be comprised of the same fundamental components, only with varying proportions, and hence the similarity index is a reliable analytical technique for determining the nature of each structure. The complex overlap within the Amide-I and Amide-II bands, in particular, can yield inflated values for the similarity index for any proteinaceous species; however the relative variations between indices is still representative of structural similarities or differences.

2.5 | Optical and EM imaging of hair cross-sections

In addition to the AFM topographical mapping of the hair cross-sections, the internal structure of hairs was also determined using both optical microscopy (Horiba LabRAM HR Evolution confocal Raman microscope, 100× objective) and scanning electron microscopy (JEOL JSM-5510LV, recorded with a secondary electron detector at ×2700 with a 10 kV beam and 19 mm working distance) of uncoated cross-sections as described above.

3 | RESULTS

3.1 | Topographical and chemical mapping

Initially, AFM-IR was used to map hair cross-sections at 1655 cm^{-1}, corresponding to the prominent Amide-I resonance of proteins. Figure 2 shows a sample AFM topographical map (A) and the corresponding IR intensity map at 1655 cm^{-1} (B) of the medulla and surrounding regions of a single, representative human hair cross-section. Two distinct constituent structures appear, namely those with an apparent larger or smaller IR intensity at 1655 cm^{-1} when compared to the surrounding cortex material. Figure 2C represents these three structures by collecting together all pixels within the map which fall within defined intensity ranges. By comparing with the height and IR maps, it is clear that the high- and low-intensity features

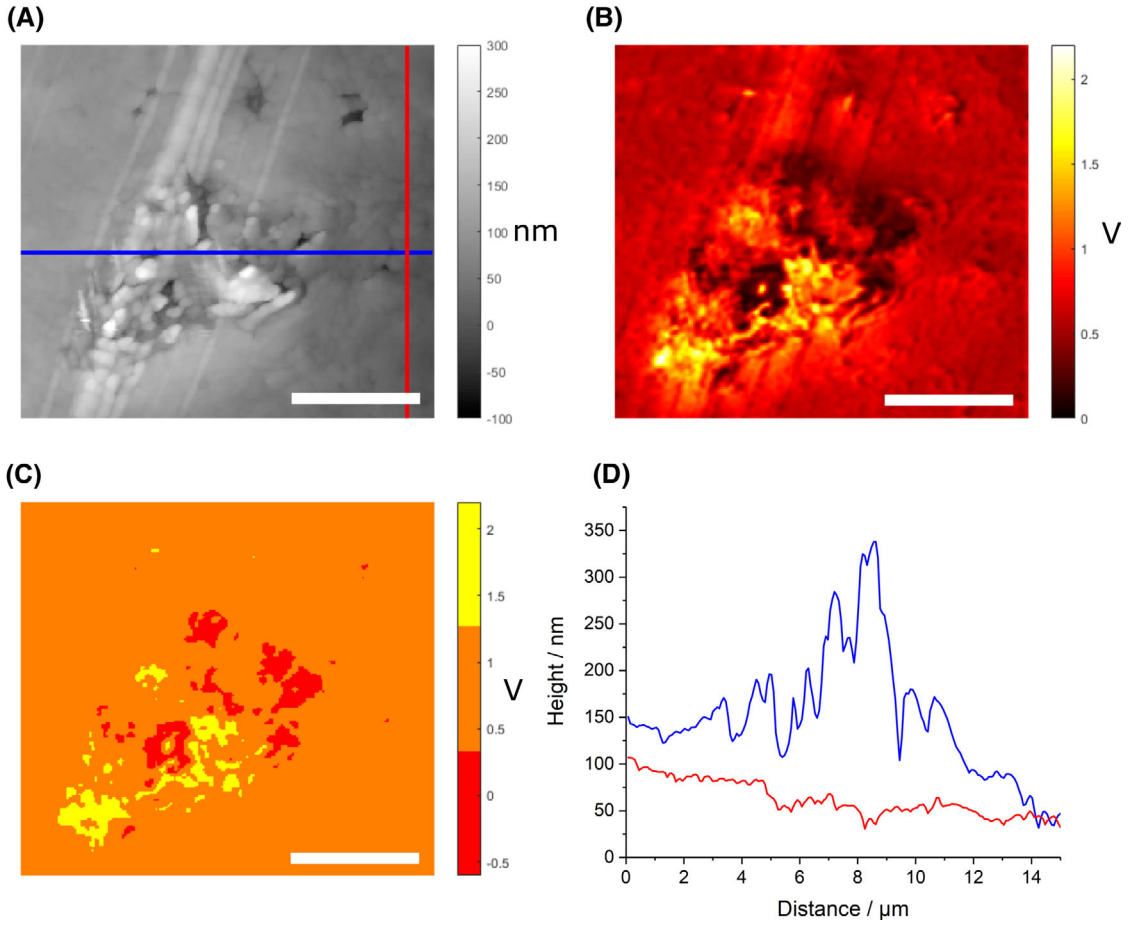

FIGURE 2 AFM-IR maps of a representative hair fibre cross-section showing (A) height topography, (B) IR intensity at 1655 cm^{-1} (scale in volts, V), (C) surface regions defined by their IR intensity at 1655 cm^{-1} (in V) and (D) example AFM height profiles across the medulla and across the cortex, as shown in the height map in (A). The scale bar represents 5 μm at the surface

predominantly fall within the medulla. The two identified medulla sub-units, corresponding to the high (yellow) and low (red) intensity features at 1655 cm^{-1} in Figure 2C, are subsequently labelled MD1 and MD2 structures respectively. The surrounding cortex material, considered to be predominantly macrofibrillar, is labelled MF (orange).

The IR intensity maps, however, are not necessarily representative of the chemical constituents within each region due to potential artefacts from tip-sample coupling and the physical properties of the different structures. This is apparent from the diagonal lines in Figure 2A and B which arise from slight imperfections introduced from sectioning. These small features are clear in the height map (Figure 2A) but also have an influence on the apparent IR intensity (Figure 2B), most likely due to alterations to the physical properties of the surface and therefore to the coupling with the tip. Furthermore, the medulla has considerably greater roughness relative to the surrounding cortex, as seen in the example of the height profile traversing the hair cross-section in Figure 2D. This is due to the large variability in physical properties (especially in their elastic moduli) of the constituents (ie both dense fibrillar structures and sparse, air-filled vacuoles), and their much less well-ordered structure, which gives rise to different behaviour when the internal stresses are released on sectioning.

These limitations can be overcome by recording ratio maps. However, biological samples such as hair, present further challenges due to the high convolution of amide bands when they arise from different protein secondary structures and specific residues. Consequently, IR maps at a frequency specific to one band can contain contributions from neighbouring bands within the spectrum owing to their proximity and bandwidth. For this reason, the IR maps shown in Figure 2 are useful only as a demonstration of different structural components within the medulla. Hence, it was essential to record localised (point) spectra to achieve chemical characterisation, and so the AFM-IR microscope images across different sections were used to identify the similar structural components, MD1, MD2 and MF, for localised spectral acquisition. Spectra of the three distinct structural regions are shown in Figure 3 (averaged

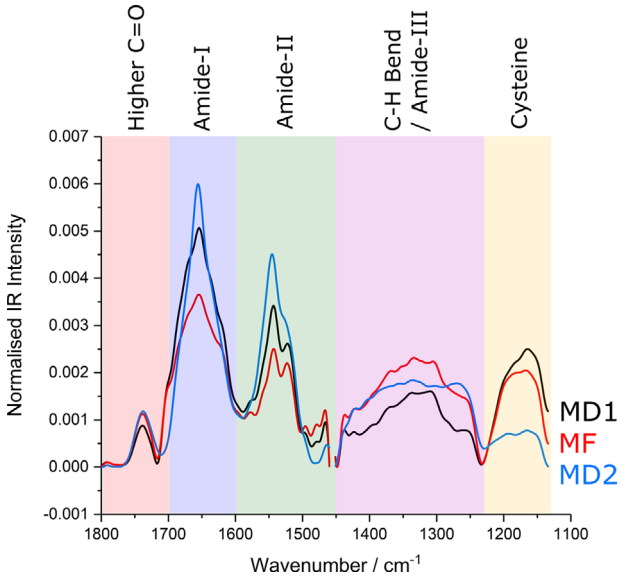

FIGURE 3 AFM-IR spectra for the two medulla structural components observed in the AFM-IR maps of Figure 2, MD1 and MD2, along with that of the surrounding cortex material dominated by macrofibrils, MF

across multiple sections from the same hair fibre, all using AFM-IR microscope images like those shown in Figure 2 to identify the three components). Although these spectra show significant differences in terms of their relative band intensities, the three structures must be formed of similar constituents since the band positions are almost constant from structure to structure. However, because the spectra show significant overlap, as previously mentioned, they must be de-convoluted to determine their chemical compositions and analyse their constituent differences.

3.2 | AFM-IR spectra: similarity indices

First, a spectral comparison of the two medulla structural components, MD1 and MD2, with that of the cortex MF species is necessary to distinguish and structurally assign them. It is clear from comparing the spectra in Figure 3 that the MD1 structure is more similar to MF than to MD2 which appears significantly different. Given that the MF is known to contain well-ordered fibrillar structures, this comparison leads to the conclusion that the MD1 structures can be assigned to the fibrillar medulla component and MD2 to the globular vacuoles, as previously revealed by EM studies. This conclusion is reinforced by the IR intensity map in Figure 2 showing considerably weaker contributions for the MD2 structures, as would be expected for regions which are essentially air-filled.

A more quantitative comparison can be made based on regression analysis of difference spectra from the different components, as shown for the Similarity Index data in Table 1 where the proportional overlap of the spectra is presented.[27] It is clear that MD1 and MF are very similar to each other (92% ± 5% overlap) while MD2 and MD1 also show a fairly significant overlap (76% ± 4%), most likely due to the vacuoles originating from similar species. In contrast, there is noticeably less similarity between MD2 and MF regions (56% ± 4% overlap). This supports the qualitative comparisons deduced from the spectral observations and provides a spectral and chemical validation of the observations from previous EM investigations[11] that is that the medulla has two distinct sub-units: one fibrillar in structure that is largely consistent with it comprising more disordered and sparse cortical cells, and the other air-filled vacuoles that show less resemblance to the fibrillar structures within the cortex.

3.3 | AFM-IR spectra: deconvolution and interpretation

From both the qualitative and quantitative spectral comparisons above, it is clear that there are significant chemical differences between the fibrillar and globular structural components within the medulla. Localised AFM-IR spectra from each of the structures can be further analysed in greater detail to characterise their specific chemistry, in an analogous fashion to that employed for bulk FTIR spectra, except that here it is on a nanometre scale. Qualitative comparisons show significant intensity differences at 1165, 1250 and 1300 cm^{-1} (Figure 3), assigned respectively to bands of cysteine oxidation products, the Amide-III protein bands, and a combination between some higher-frequency Amide-III bands with C-H and C-C bands dominated by Tryptophan.[28,32–39] Nevertheless, although there are differences in the intensities of the MD1 and MF structures, their spectral profiles are notably similar, suggesting similar chemical structures. In contrast there are significant differences with the MD2 structure, the most notable of which is the large reduction in the intensity of the cysteine oxidation product region compared to other protein-related bands (ie Amide-I, -II and -III), indicating a much-reduced concentration of cysteine oxidation products in the MD2 structure. The other spectral differences are mostly in the band-shapes, which can be attributed to differences in the respective contributions from underlying bands. This points to different amounts of constituent proteins within the MD2 structure with a variety of chemical structures and/or conformations.

From the α-helix protein secondary structure of the Amide-I band at ~1655 cm^{-1}, it can be seen that the MD2 structures have increased intensity relative to those

TABLE 1 Calculated similarity indices, using difference spectra regression, between the two medulla species MD1 and MD2 also with the cortex (MF) giving the proportional overlap. Uncertainties were calculated using the apparent noise level within the difference spectra

Similarity index	MD1	MD2	MF
MD1	1	–	–
MD2	0.76 ± 0.04	1	–
MF	0.92 ± 0.05	0.56 ± 0.04	1

of the MD1 and MF features and, correspondingly, have, from the intensity at ~1610-1640 cm^{-1}, less β-sheet protein. A similar observation can be concluded from the Amide-II band which has prominent features at ~1525 and 1545 cm^{-1} from the α-helix and β-sheet proteins, respectively, that show a similar intensity relationship. However, due to the convoluted nature of these spectral regions, firm structural conclusions are not always forthcoming from facile spectral comparisons and the bands must be deconvoluted, the common practise used in the spectral analysis of proteinaceous materials. Therefore, to derive conclusions beyond these qualitative comparisons of well-known and prominent band features (ie α-helices and β-sheets) requires deconvolution. The main spectral regions considered for deconvolution are those of the Amide-I and Amide-II bands (Figure 3) which contain significantly overlapping contributions that are characteristic of the constituent protein structures and environments. After deconvolution, the contributing bands can be assigned to the different protein structures and amino acid residues present in each species.

Figure 4 shows both the fitted spectra (left panel) and their corresponding second derivatives (right panel) for the three identified components MD1 (top), MD2 (middle) and MF (bottom). The band origins appear as minima in the second derivative spectra. Particular care was taken to eliminate artificially improving the fit by including additional bands. In order to increase the reliability of the fit, high-quality spectra were recorded and filtered for atmospheric corrections without perturbing the underlying band structure. The second derivative spectra then provided the band origins for comparisons with known values from the literature which was used to test the robustness of the procedure. After fitting, the band intensity profile of each structure can readily be calculated using the fitted areas. Greater detail on deconvolution procedures can be found elsewhere in the literature as well as in the experimental section.[26–28,40] The intensity profiles based on the deconvoluted spectra in Figure 4 can be found in Figure 5 where three separate spectral regions (Amide-II, Amide-I and >1700 cm^{-1}) have been separated from each other and normalised independently (the bands >1700 cm^{-1} are also shown in the Amide-I profiles for comparison). These profiles, along with the assignments given in Table 2 from the literature,[41–45] can be used to analyse the variations in contributing species for each of the features investigated and as discussed in the following sections.

i. Amide-II

The two bands at 1462 (band 1) and 1480 cm^{-1} (band 2) are both associated with aliphatic C-H deformation modes but from different environments namely lipid/triglyceride tail groups or aliphatic amino acid residues within the protein network. While these bands have a qualitatively similar intensity in the MD1 and MF structures, they are more intense in MF, indicating a greater presence of aliphatic species in the cortex. In the MD2 structure, the relative intensity of the two bands is reversed, that is there is a significant change in the concentrations of the contributing species. Furthermore, although their spectra are broadly similar, there is a noticeable change in the band ratio between MD1 and MF, supporting the conclusion of a greater overall lipid contribution from the medulla.

The band at 1495 cm^{-1} corresponds to the C-N in-ring stretching mode arising predominantly from the His/Trp residues.[43,44] This feature appears uniformly across the different medulla components but with a greater intensity in the cortex, indicating there is a lower amount within the medulla. This agrees with results in the literature where these species are reported to be significant in the cortex.[32,46]

Bands 4 and 5 in Table 2 correspond to the β-sheet protein secondary structures of the Amide-II band in antiparallel and parallel configurations respectively.[28,33,34,41,42] Both bands show virtually uniform intensity across all three regions suggesting very little difference in the relative proportions of β-sheets throughout. There is a slight increase in the antiparallel to parallel ratio going from MD1 to MF to MD2 which is indicative of the extent of conformational restriction on the protein structures since the antiparallel conformer is the thermodynamically most stable conformer. Hence, this suggests increased and decreased cross-linking within the MD1 and MD2 regions compared to the cortex respectively. This is reflected in the significantly lower relative cysteine-related contribution in the MD2 spectra (Figure 3) and correlates with a loss of matrix-like material in this structure.

Band 6 originates from the combination of α-helices and random-coil proteins and shows large differences in the

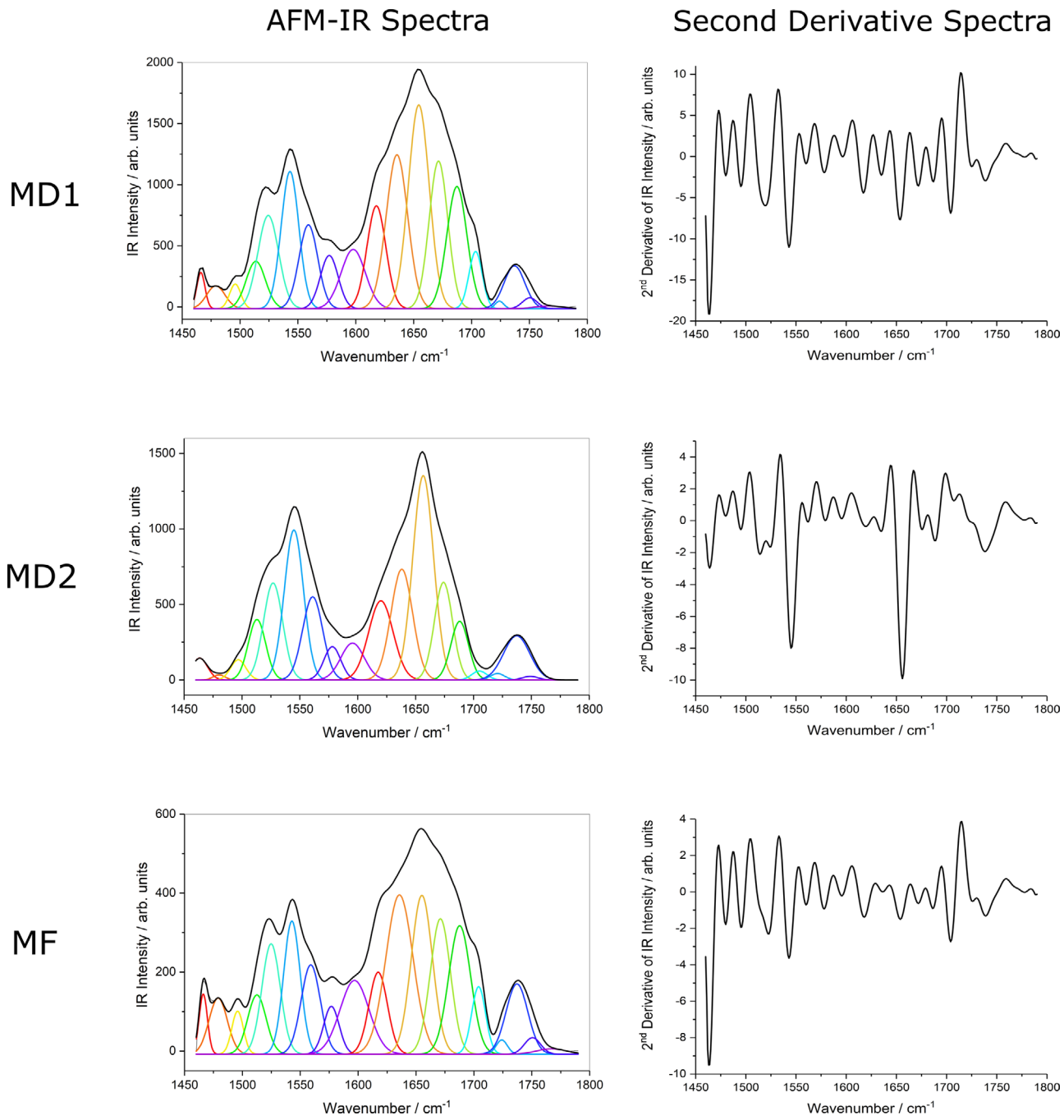

FIGURE 4 AFM-IR analysis of the two medulla components, MD1 (top) and MD2 (middle), as well as the surrounding microfibrillar cortex material, MF (bottom), as identified in AFM-IR microscope images (eg Figure 2). Left panel: Smoothed AFM-IR spectra, baseline-corrected using a spline curve, and fitted with constituent bands identified using the second and fourth derivatives of the smoothed spectra. Right panel: Second derivative spectra of the AFM-IR spectra shown in the left panel with minima indicating contributing band centres

three components: greatest in MD2 and least in MF.[34–36,41] Since this band is a combination of two types of secondary structure, no further assignment can be made without a comparison with other bands from these secondary structures (ie in the Amide-I region). The major contribution to band 7 is the Trp CH_2 tri-substituted indole ring vibration with a similar intensity for MD1 and MF but tending towards a larger proportion in MD2.[41,44] The behaviour of this band may be compared with the uniform distribution across all three structures observed for band 3, a combination of His and Trp vibrations. As Trp is in greater proportion in MD2 conversely this indicates a lower proportion of His in this structure. Band 8 is mainly due to the antisymmetric COO^- stretch of deprotonated acidic

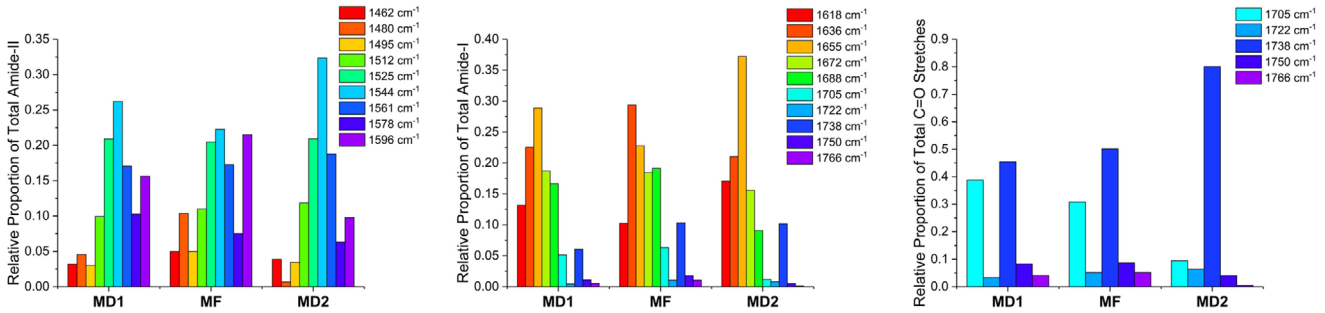

FIGURE 5 Band profiles in block format for the deconvoluted spectra of the two medulla components, MD1 and MD2, along with the macrofibrillar cortex, MF. The profiles shown are for the Amide-II region (left), Amide-I region including the C = O bands above 1700 cm^{-1} (centre) and C = O region > 1700 cm^{-1} (right). All profiles have been normalised separately from their constituent bands (where the bands >1700 cm^{-1} have not been included in the Amide-I region normalisation)

TABLE 2 Band origins determined using the derivative spectra for the MD1, MD2 and MF features, showing any band-origin differences. The assignments are based on data available in the literature

	MD1	MD2	MF	Assignment
Amide-II				
Band 1	1462	1463	1462	Aliphatic C-H def.
Band 2	1480	1480	1480	Aliphatic C-H def.
Band 3	1495	1496	1495	His/Trp C-N str. (in ring)
Band 4	1513	1512	1512	β-sheet (AP)
Band 5	1524	1527	1525	β-sheet (P)
Band 6	1543	1545	1543	α-helix/random coil
Band 7	1560	1562	1560	Trp (indole ring vibration)
Band 8	1578	1579	1577	Asp/Glu COO^- str. (AS)
Band 9	1597	1595	1596	His/Tyr/Trp C-C str. (in ring)
Amide-I				
Band 10	1617	1619	1617	β-sheet (AP)
Band 11	1635	1637	1636	β-sheet (P)
Band 12	1654	1656	1654	α-helix
Band 13	1671	1674	1672	β-turn
Band 14	1687	1689	1687	Asp/Glu amide str. or β-sheet
Higher carbonyls				
Band 15	1704	1706	1705	C=O (H-bonded acidic residue)
Band 16	1723	1721	1723	C=O ('Free' acidic residue)
Band 17	1738	1737	1738	C=O (lipid/triglyceride ester)
Band 18	1751	1748	1751	C=O (monomeric acidic residue)
Band 19	1766	1766	1766	C=O (monomeric acidic residue)

residues and is most prominent in MD1, with similar intensities for MF and MD2.[41] The last band of the Amide-II region (band 9, 1596 cm^{-1}) shows large differences across the three structures. This band is attributed to a combination of His, Trp and Tyr residues and, due to band overlap from many sources, further assignment is not feasible. Tyrosine has previously been shown to be in greater concentrations in the medulla so the cortex MF component showing the strongest contribution indicates that the contribution to this band from tyrosine is likely to be minimal.[46]

ii. Amide-I

The Amide-I region starts at bands 10 and 11 at 1618 and 1636 cm^{-1} from the antiparallel and parallel β-sheet conformers respectively (Table 2).[33,41,42,45] Although they contribute significantly to the Amide-II region, their bands

show large homogeneity between MD1 and MD2, the two different medulla components, as well as the surrounding cortex, MF. As previously mentioned, this is most likely to be due to the Amide-II region containing many overlapping contributions including plausible contributions from ring vibrational modes which could contribute differently to the constituent bands.[37–39,47,48] In the MF component, the parallel β-sheet form (band 11) dominates (cf. band 10) whereas in the MD2 structures it is much less in evidence. In MD1, the relative intensity of the parallel form lies between these two extremes. The antiparallel arrangement is known to be slightly more stable due to facile H-bonding and so the species that show the greatest relative proportion of the antiparallel arrangement are thought to correspond to a more stable environment and more freedom for the structures to rearrange.[49] This conformational freedom is commonly negatively correlated with restrictive intermolecular interactions, for example crosslinking from cysteine-related residues, increasing the energy barrier to rearrangements.[33]

The third band (band 12) of the Amide-I region is the α-helix band (1655 cm^{-1}) that is most prevalent in the MD2 structure and lowest in MF.[34,41,42,45] The profile of this band can be compared to that of the 1544 cm^{-1} band in the Amide-II region which arises mainly from a combination of the α-helix conformer with randomly coiled proteins. Both of these band profiles show the same variation across the different structures which indicates a uniform (or small) distribution of random coils throughout and that variations are dominated by that of the α-helix conformers. Like the cortex, based on the profile of the α-helix band, the different components in the medulla also show significant proportions of this protein secondary structure. Although MF shows the lowest proportion of α-helices there is likely to be some contribution from matrix material rather than just the intermediate filaments (predominantly α-helical in structure), hence yielding an intrinsically weaker α-helical presence. This is because the matrix material is highly proteinaceous and houses significant β and some random coil protein structures. This, therefore, suggests that there is a less 'matrix-like' material constituent to the medulla and a greater presence of fibrillar material.

Band 13 at 1672 cm^{-1} primarily arises from β-turn secondary structures with similar proportions for MD1 and MF but is notably lower for the MD2 structure. This band is usually associated with more randomly oriented protein networks owing to the presence of significant turning points and kinks in the chains.[50,51] This contribution is of greater significance in the intermacrofibrillar matrix compared to the macrofibrils of the cortex, due to differences in the protein structures in the two components. Hence, the lower contribution in MD2 found here supports the proposal of lesser 'matrix-like' material in these structures. The final band in the Amide-I region at 1688 cm^{-1} is from the amide side chain of Asparagine and Glutamine residues.[41] This band is strongest in MF and weakest in MD2, thereby indicating the relative proportions of amide side chains in each structure.

iii. Carbonyl bands >1700 cm^{-1}

Spectral deconvolution reveals five bands above 1700 cm^{-1} that can be assigned to the carbonyl vibrations in acidic amino acid side chains (mainly Asp and Glu) and ester moieties in any lipids and triglycerides that may be present.[28,40,52,53] The two lowest frequencies at 1705 and 1722 cm^{-1} arise from different states of association of dimer-like acid groups and most likely originate from carboxylic acid side chains of Asp and Glu residues.[52,54] These are both doubly H-bonded but to different extents where the lower frequency band comes from the stronger H-bond.[54] When considered together, these two bands provide an indication of the total protonated acidic species in dimer form present in each component. It is clear that MD2 has considerably lower concentrations than other structures. Relative to the Amide-I region, the sum of the intensity of these two bands show an increased intensity for MF compared to MD1. Their intensity is, however, reversed when compared to the intensity of the complete carbonyl region >1700 cm^{-1}. This demonstrates the importance of signal normalisation and, given that acidic residues are associated with proteins, normalisation to the Amide-I region is appropriate. Hence, the intensity reversal when comparing to the >1700 cm^{-1} bands indicates that there must be significant contributions from non-proteinaceous sources within this spectral region.

Band 17 at 1738 cm^{-1} has significant intensity and is assigned to ester functions of lipids and triglycerides. Due to the large lipid contribution, the bands from acidic protein residues (eg Asp and Glu) will be significantly affected if normalised relative to the bands above 1700 cm^{-1} rather than the protein Amide-I contributions. Additionally, since the lipids and triglycerides are commonly associated with the protein structures (eg stabilisation through structural lipids), it is also logical to compare their intensity to that of the total protein content, that is, that of the Amide-I region. Using this normalisation, the biggest contribution from bands >1700 cm^{-1} is in the MF structure. An interesting result arises from examining the relative intensity of the two bands at 1705 and 1722 cm^{-1} (as discussed above) which shows a more pronounced strongly bound band (1705 cm^{-1}) in MD1 than in MD2 meaning that stronger interactions are more common in the former component. The lipid ester band at 1738 cm^{-1} (band 17) has greater abundance in the MF and MD2 structures and with similar intensities to the Amide-I region. However,

relative to the total intensity of the carbonyl region above 1700 cm^{-1}, there is a much greater proportion of the lipid in the MD2 component. Therefore, due to the presence of the strong lipid band, comparison of the acidic residue contributions is most valuable when normalised to the Amide-I intensity, but determination of the lipid concentration is most meaningful through normalisation of the contributions >1700 cm^{-1}. Hence, it is reasonable to conclude that the MD2 structure shows a stronger presence of lipid than the MD1 structure or the cortex (MF) as well as considerably less strongly bound acidic protein residues. The highest frequency (weak) bands above 1700 cm^{-1}, 1750 (band 18) and 1766 cm^{-1} (band 19), are assigned to monomeric carboxylic acid groups, once again primarily from the acidic Asp and Glu side chains.[40,52,54] These same bands are frequently observed for carboxylic acid species in the condensed phase where dimer H-bonding is disrupted by H-bonding with solvent molecules.[52,55] Unlike the dimeric species and bands described above, they are considered to form fewer H-bonds per molecule, hence their higher stretching frequencies.[54] The two contributions arise from different degrees of H-bonding with the lower frequency band participating in stronger interactions and the higher frequency band corresponding to a 'free' vibration. The total intensity from these monomeric species is greatest in MF and lowest in the MD2 structure, as observed for the dimer species. This is consistent with the variations being due to overall acidic Asp and Glu species concentrations rather than significant variations in the dimer to monomer ratio. The relative ratio of the two monomer bands, however, is variable with the preponderance for strongly bound species occurring in the order: MD2 > MD1 > MF. This contrasts significantly with the association of the dimeric species where the MD2 structure is the least preponderant for strongly bound species.

4 | DISCUSSION

Initial AFM-IR topographical and spectroscopic mapping clearly identified 3 distinct structures, two of which solely reside in the medulla (MD1 and MD2), and one surrounding material (MF). Both qualitative and quantitative (by means of similarity indices) comparisons between localised spectra from these three structures clearly showed great similarity between MD1 and MF, with MD2 having significant chemical differences. From this analysis, along with the AFM-IR mapping, it was evident that there is significant spectroscopic support for the conclusions based on prior EM investigations, namely that the MD1 and MD2 medulla components are the fibrillar and globular structures assigned to randomly oriented cortical cells and vacuoles, respectively.

Further qualitative visual comparisons of the individual spectra showed a reduction in cysteine-related products in the vacuoles (MD2 structures) as well as the amide band shapes indicating an apparent increase in the proportion of α-helix protein compared to the β-sheet secondary structures for the vacuoles compared with the fibrillar structures (MD1) and surrounding cortex. This observation was confirmed by spectral deconvolution of the amide and higher carbonyl regions which allowed for a more in-depth comparison of the chemical constituents.

As shown from the results in Figures 4 and 5, in comparison to the other components, the vacuoles (MD2 structures) show greater contributions from lipids, α-helix proteins, antiparallel β-sheet proteins (cf. parallel β-sheet proteins) as well as strongly associated, monomeric acidic side chains. Conversely, there are reduced amounts of overall β-sheet proteins, parallel β-sheet proteins (cf. antiparallel β-sheet proteins), β-turn proteins, overall concentrations of acidic residues as well as the strongly bound 'dimeric-like' acid residues. The increase in α-helices relative to β-sheets compared to the two fibrillar structures was surprising given the fibrillar vs. globular nature of these structures. However, this was attributed to a loss of 'matrix-like' material in the vacuoles since the matrix contains large proportions of β-sheets and is a significant component of cortical cells. The observation of lower concentrations of cysteine-related products in the vacuoles is also consistent with the less 'matrix-like' material present in this component.[1] Because the essentially empty vacuoles do not contain much 'matrix-like' material, the spectral contributions will come predominantly from the 'shell' of the vacuole.

The increased proportion of structural lipids within the vacuoles (MD2) compared to the cortical cells (MF) is consistent with earlier observations which showed greater lipid content in the medulla than in the cortex. However, as the MD1 component shows a proportionately lower contribution relative to the cortex, it suggests that the majority of the structural lipid within the medulla must be located within the vacuoles.[25] These structural lipids are likely to be involved in the protein network through associative interactions to stabilise the protein structures. This conclusion is consistent with the vacuoles (MD2) having lower contributions from acidic residues compared to the cortex as these amino acid moieties are known to stabilise protein conformers (particularly α-helices) through H-bonding.[56,57] Hence, structural lipid stabilisation is likely to compete with H-bonding from these amino acid side chains. Increased lipid stabilisation is also suggested by comparing the relative proportion of strongly bound 'dimeric-like' acid species to the 'free' species, which is lower in the vacuoles (MD2) than in the cortex.

Additional consideration must be given to citrulline that is believed to bind the fibrillar structures to the vacuoles through peptide linkages and hence would also be expected to H-bond and stabilise the protein network, thereby also competing with the acidic residues.[17] The interactions between the protein residues resulting in stabilisation of the protein structures will yield dimeric H-bonded acid groups whereas stabilisation by other means, for example structural lipid association, will result in these H-bonds being displaced. Thus, increased proportions of monomeric acid species within the vacuoles (MD2) compared to the cortex is indicative of greater stabilisation through lipid interactions. A further consideration is that the greater relative proportion of strongly bound monomeric species to the 'free' species suggests that the residues that have H-bonds displaced by lipid interactions are intermolecularly stabilised through other sources of H-bonding.

The protein network within the vacuoles is dominated by α-helix structures which are probably stabilised by structural lipids and some associative interactions with Citrulline and Asp and Glu (acidic) residues as previously discussed. This is consistent with the suggested reduction in 'matrix-like' material within the vacuoles which is signified by the lower β-turn concentrations associated with more organised proteins. Additionally, the more stable antiparallel β-sheets are more prevalent here which is, as we have commented on earlier, indicative of protein networks that have more freedom to rearrange to form more thermodynamically stable structures. This is compatible with the lower cysteine content found in this region suggesting much reduced cross-linking and hence a less-restricted network.

5 | CONCLUSION

In this study, AFM-IR has been used to physically and chemically distinguish the different sub-structures within the medulla of human hair fibres. In agreement with previous results, topographical maps showed that the medulla exhibits significant disorder, containing randomly oriented structures. Spectroscopic mapping of these structures indicated large differences in IR intensity, identifying two components to the medulla, as suggested in previous EM investigations. Comparisons of localised spectra from each structure confirmed the chemical distinction of the two components. Specifically, similarity index calculations of the spectra from these two structures and the surrounding cortex showed significant similarity between one of the two observed medulla components and the macrofibrils, the other component being largely different to both. These observations corresponded well to the previously suggested composition consisting of fibrillar cells and globular vacuoles. This provides strong evidence for the proposed nature of the medulla constituents, namely that the fibrillar structures are essentially randomly oriented cortical-like cells and the other component, presenting broadly with low IR intensity, is attributed to the air-filled globular structures and vacuoles that have previously been suggested to form the main medulla sub-unit. Further spectral analysis of these globular vacuoles showed that they possessed comparatively low cysteine concentrations and the greatest proportion of the most thermodynamically stable antiparallel β-sheet protein structures, indicating greater protein spatial freedom. This freedom chimes with the observed low cysteine content which can restrict the protein network through extensive disulphide cross-links. The vacuoles also showed the least Asp/Glu acidic residues, in both dimer- and monomer-like entities, suggesting a lack of the protein stability they could provide through H-bonding. However, protein stabilisation can also be provided by structural lipids which are abundant within the medulla, with particularly large concentrations in the globular structures. The α-helix conformers were shown to also be in considerably greater concentrations in the vacuoles than in the fibrillar structures, suggesting that the latter are highly thermodynamically favourable. There is likely to be competition between the H-bonding moieties present such as the structural lipids and acidic side-chain amino-acid residues. For the vacuoles, therefore, the evidence points to the structural lipids providing the dominant interactions whereas for the fibrillar structures and the cortex, the stability of the protein structures originates mostly through the acidic residues.

ACKNOWLEDGEMENTS

We are grateful to Dr Paul Pudney and Dr Ken Lee at Unilever R&D for providing support and guidance through the project. Additionally, we are thankful for Unilever R&D and the EPSRC for providing the iCASE studentship for APF on Grant EP/R511870/1.

CONFLICT OF INTEREST

There are no conflicts to declare.

ORCID

Alexander P. Fellows https://orcid.org/0000-0002-5885-8144

REFERENCES

1. Robbins, C. R. (2012). *Chemical and physical behavior of human hair* (5th edn.), Berlin, Heidelberg: Springer-Verlag.
2. Cena, K., & Clark, J. A. (1978). Thermal insulation of animal coats and human clothing. *Physics in Medicine and Biology*, *23*, 565–591.

3. Randall, V. A. (2007). Hormonal regulation of hair follicles exhibits a biological paradox. *Seminars in Cell & Developmental Biology*, *18*, 274–285.
4. Draelos, Z. K. (1995). Cosmetics: An overview. *Current Problems in Dermatology*, *7*, 45–64.
5. Trüeb, R. M. (2001). The value of hair cosmetics and pharmaceuticals. *Dermatology*, *202*, 275–282.
6. Miao, M., & Xin, J. H. (2017). *Engineering of high-performance textiles*. Duxford, UK: Elsevier.
7. Harrison, S., & Sinclair, R. (2003). Hair colouring, permanent styling and hair structure. *Journal of Cosmetic Dermatology*, *2*, 180–185.
8. Yang, F. C., Zhang, Y., & Rheinstädter, M. C. (2014). The structure of people's hair. *PeerJ*, *2014*, e619.
9. Dias, M. F. R. G. (2015). Hair cosmetics: An overview. *International Journal of Trichology*, *7*, 2–15.
10. Robbins, C. R. (2009). The cell membrane complex: Three related but different cellular cohesion components of mammalian hair fibers. *Journal of Cosmetic Science*, *60*, 437–465.
11. De Cássia Comis Wagner, R., Kiyohara, P. K., Silveira, M., & Joekes, I. (2007). Electron microscopic observations of human hair medulla. *Journal of Microscopy*, *226*, 54–63.
12. Wagner, R., & Joekes, I. (2007). Hair medulla morphology and mechanical properties. *Journal of Cosmetic Science*, *58*, 359–368.
13. Kreplak, L., Briki, F., Duvault, Y., Doucet, J., Merigoux, C., Leroy, F., … Dumas, P. (2001). Profiling lipids across Caucasian and Afro-American hair transverse cuts, using synchrotron infrared microspectrometry. *International Journal of Cosmetic Science*, *23*, 369–374.
14. Deedrick, D., & Koch, S. (2004). Microscopy of hair part II: A practical guide and manual for animal hairs. *Forensic Science Communications*, *6*, 1–20.
15. Moorthy T, N., & Roy, J. M. (2015). Study on hair morphology to distinguish the dominant races in Malaysia for forensic investigation. *Journal of Forensic Science & Criminology*, *3*, 403.
16. Chernova, O. F. (2014). Scanning electron microscopy of the hair medulla of orangutan, chimpanzee, and man. *Doklady Biological Sciences*, *456*, 199–202.
17. Clement, J. L., Pareux, A. L.e, & Ceccaldi, P. F. (1981). Contribution a L'Etude De La Medulla Des Poils. *Annales De Dermatologie Et De Venereologie*, *108*, 849–857.
18. Dazzi, A., & Prater, C. B. (2017). AFM-IR: Technology and applications in nanoscale infrared spectroscopy and chemical imaging. *Chemical Reviews*, *117*, 5146–5173.
19. Dazzi, A., & Prater, C. B. (2017). AFM-IR: Technology and applications in nanoscale infrared spectroscopy and chemical imaging. *Chemical Reviews*, *117*, 5146–5173.
20. Ruggeri, F. S., Marcott, C., Dinarelli, S., Longo, G., Girasole, M., Dietler, G., & Knowles, T. P. J. (2018). Identification of oxidative stress in red blood cells with nanoscale chemical resolution by infrared nanospectroscopy. *International Journal of Molecular Sciences*, *19*, 1–14.
21. Goussous, S. A., Fellows, A. P., Casford, M. T. L., & Davies, P. B. (2019). A time domain study of surfactin penetrating a phospholipid monolayer at the air-water interface investigated using sum frequency generation spectroscopy, infrared reflection absorption spectroscopy, and AFM-nano infrared microscopy. *Biochimica et Biophysica Acta– Biomembranes*, *1861*, 1568–1578.
22. Fellows, A. P., Puhan, D., Casford, M. T. L., & Davies, P. B. (2020). Understanding the lubrication mechanism of poly(vinyl alcohol) hydrogels using infrared nanospectroscopy. *Journal of Physical Chemistry C*, *124*, 18091–18101.
23. Fellows, A. P., Casford, M. T. L., & Davies, P. B. (2020). Infrared nanospectroscopy of air-sensitive biological substrates protected by thin hydrogel films. *Biophysical Journal*, *119*, 1474–1480.
24. Fellows, A. P., Casford, M. T. L., Davies, P. B., Gibson, J. S., Brewin, J. N., & Rees, D. C. (2021). Nanoscale adhesion profiling and membrane characterisation in sickle cell disease using hybrid atomic force microscopy-IR spectroscopy. *Colloids Surfaces B Biointerfaces*, 197, 111383. https://doi.org/10.1016/j.colsurfb.2020.111383.
25. Marcott, C., Lo, M., Kjoller, K., Fiat, F., Baghdadli, N., Balooch, G., & Luengo, G. S. (2014). Localization of human hair structural lipids using nanoscale infrared spectroscopy and imaging. *Applied Spectroscopy*, *68*, 564–569.
26. Fellows, A. P., Casford, M. T. L., & Davies, P. B. (2020). Nanoscale molecular characterization of hair cuticle cells using integrated atomic force microscopy–infrared laser spectroscopy. *Applied Spectroscopy*, *74*, 1540–1550.
27. Fellows, A. P., Casford, M. T. L., & Davies, P. B. (2020). Spectral analysis and deconvolution of the amide I band of proteins presenting with high-frequency noise and baseline shifts. *Applied Spectroscopy*, *74*, 597–615.
28. Barth, A. (2007). Infrared spectroscopy of proteins. *Biochimica et Biophysica Acta (BBA)—Bioenergetics*, *1767*, 1073–1101.
29. Yang, H., Yang, S., Kong, J., Dong, A., & Yu, S., Obtaining information about protein secondary structures in aqueous solution using Fourier transform IR spectroscopy. *Nature Protocols*, https://doi.org/10.1038/nprot.2015.024.
30. Byler, D. M., & Susi, H. (1986). Examination of the secondary structure of proteins by deconvolved FTIR spectra. *Biopolymers*, *25*, 469–487.
31. Holler, F., Burns, D. H., & Callis, J. B. (1989). Direct use of second derivatives in curve-fitting procedures. *Applied Spectroscopy*, *43*, 877–882.
32. Bertazzo, A., Biasiolo, M., Costa, C. V. L., Cardin de Stefani, E., & Allegri, G. (2000). Tryptophan in human hair: Correlation with pigmentation. *Farmaco*, *55*, 521–525.
33. Litvinov, R. I., Faizullin, D. A., Zuev, Y. F., & Weisel, J. W. (2012). The α-helix to β-sheet transition in stretched and compressed hydrated fibrin clots. *Biophysical Journal*, *103*, 1020–1027.
34. Zhang, G., Senak, L., & Moore, D. J. (2011). Measuring changes in chemistry, composition, and molecular structure within hair fibers by infrared and Raman spectroscopic imaging. *Journal of Biomedical Optics*, *16*, 056009.
35. Aisenbrey, C., Kinder, R., Goormaghtigh, E., Ruysschaert, J. M., & Bechinger, B. (2006). Interactions involved in the realignment of membrane-associated helices: An investigation using oriented solid-state NMR and attenuated total reflection Fourier transform infrared spectroscopies. *Journal of Biological Chemistry*, *281*, 7708–7716.
36. Brasseur, R. (2018). *Molecular description of biological membranes by computer aided conformational analysis*. Boca Raton, Florida: CRC Press.
37. Vedantham, G., Sparks, H. G., Sane, S. U., Tzannis, S., & Przybycien, T. M. (2000). A holistic approach for protein secondary structure estimation from infrared spectra in H2O solutions. *Analytical Biochemistry*, *285*, 33–49.

38. Cai, S., & Singh, B. R. (2004). A distinct utility of the amide III infrared band for secondary structure estimation of aqueous protein solutions using partial least squares methods. *Biochemistry*, *43*, 2541–2549.
39. Combs, J. D., Gonzalez, C. U., & Wang, C. (2016). Surface FTIR techniques to analyze the conformation of proteins/peptides in H2O environment. *Journal of Physical Chemistry & Biophysics*, *6*, 1000202.
40. Barth, A. (2000). The infrared absorption of amino acid side chains. *Progress in Biophysics and Molecular Biology*, *74*, 141–173.
41. Barton, P. M. J. (2011). A forensic investigation of single human hair fibres using FTIR-ATR spectroscopy and chemometrics. PhD Thesis, Queensland University of Technology, Brisbane.
42. Panayiotuo, H. (2004) Vibrational spectroscopy of keratin fibres: A forensic approach. PhD Thesis, Queensland University of Technology, Brisbane.
43. Epishina, L. V., Slovetskii, V. I., Osipov, V. G., Lebedev, O. V., Khmel'nitskii, L. I., Sevost'yanova, V. V., & Novikova, T. S. (1969). Infrared spectra and the structure of salts of imidazoles. *Chemistry of Heterocyclic Compounds*, *3*, 570–575.
44. Rao, C. N. R., & Venkataraghavan, R. (1964). Contribution to the infrared spectra of five-membered N- and N,S-heterocyclic compounds. *Canadian Journal of Chemistry*, *42*, 43–49.
45. Kong, J., & Yu, S. (2007). Fourier transform infrared spectroscopic analysis of protein secondary structures. *Acta Biochimica et Biophysica Sinica*, *39*, 549–559.
46. Robbins, C. R. (2012). Chemical Composition of Different Hair Types. *Chemical and physical behavior of human hair* (pp. 105–176). Berlin, Heidelberg: Springer-Verlag.
47. Fabian, H., & Mäntele, W. (2006). Infrared Spectroscopy of Proteins. *Handbook of vibrational spectroscopy*. J. M. Chalmers, and P. R. Griffiths, (Eds.) (pp. 2999–3454). Hoboken, NJ: John Wiley & Sons Ltd.
48. Fayer, M. D. (2013). *Ultrafast infrared vibrational spectroscopy*. M. D. Fayer, (Ed.) (pp. 1–33), Boca Raton, Florida: CRC Press.
49. Kobayashi, K., Granja, J. R., & Ghadiri, M. R. (1995). β-Sheet peptide architecture: Measuring the relative stability of parallel vs. antiparallel β-sheets. *Angewandte Chemie*, *34*, 95–98.
50. Ishizaki, H., Balaram, P., Nagaraj, R., Venkatachalapathi, Y. V., & Tu, A. T. (1981). Determination of beta-turn conformation by laser Raman spectroscopy. *Biophysical Journal*, *36*, 509–517.
51. Ball, J. B., Hughes, R. A., Alewood, P. F., & Andrews, P. R. (1993). β-turn topography. *Tetrahedron*, *49*, 3467–3478.
52. Flett, M. S. C. (1951). The characteristic infra-red frequencies of the carboxylic acid group. *Journal of the Chemical Society*, *1951*, 962–967.
53. Mihály, J., Deák, R., Szigyártó, I. C., Bóta, A., Beke-Somfai, T., & Varga, Z. (2017). Characterization of extracellular vesicles by IR spectroscopy: Fast and simple classification based on amide and C[sbnd]H stretching vibrations. *Biochimica et Biophysica Acta–Biomembranes*, *1859*, 459–466.
54. Nie, B., Stutzman, J., & Xie, A. (2005). A vibrational spectral maker for probing the hydrogen-bonding status of protonated Asp and Glu residues. *Biophysical Journal*, *88*, 2833–2847.
55. Feughelman, M. (2019). Physical properties of hair. *Hair and hair care*. D. H. Johnson, (Ed.) (pp. 13–32). New York: Routledge.
56. Berg, J. M., Tymoczko, J. L., & Stryer, L. (2002). *Biochemistry*. New York: W. H. Freeman and Company, p. Section 3.3.
57. Cruz, C. F., Costa, C., Gomes, A. C., Matamá, T., & Cavaco-Paulo, A. (2016). Human hair and the impact of cosmetic procedures: A review on cleansing and shape-modulating cosmetics. *Cosmetics*, *3*, 26.

How to cite this article: Fellows AP, Casford MTL, Davies PB. Using hybrid atomic force microscopy and infrared spectroscopy (AFM-IR) to identify chemical components of the hair medulla on the nanoscale. *Journal of Microscopy*. 2021;1–14. https://doi.org/10.1111/jmi.13052